Radiation Physics and Chemistry 80 (2011) 1119

Structural and magnetic properties of Mn^+ implanted silicon crystals studied using X-ray absorption spectroscopy techniques

A. Wolska [a,*], M.T. Klepka [a], K. Lawniczak-Jablonska [a], A. Misiuk [b] and D. Arvanitis [c]

[a] *Institute of Physics PAS, al. Lotnikow 32/46, PL-02-668 Warsaw, Poland*
[b] *Institute of Electron Technology, al. Lotnikow 46, PL-02-668 Warsaw, Poland*
[c] *Physics Department, Uppsala University, Box 530, 75121 Uppsala, Sweden*

*corresponding author:
wolska@ifpan.edu.pl
tel: (+48) 22 843 6601 ext. 3348
fax: (+48) 22 843 6034

Abstract

The implantation of Mn ions into two Si substrates with different doping (P or B), resistivity and oxygen content was performed at the low and high substrate temperatures. Different post implantation processing was carried out to study its influence on the structural and magnetic properties of these samples. The local order around the Mn atoms was characterized by X-ray absorption fine structure techniques and the magnetic properties of the Mn ionic cores were determined by means of X-ray magnetic circular dichroism measurements. The results are discussed in relation to the structural and macroscopic magnetic properties. It is shown that the amorphous matrix speeds up the formation of $MnSi_x$ inclusions. However, the existence of inclusions or the type of electrically active dopants is not directly related to the magnetic properties. Therefore, in the performed studies, the importance of structural defects on the magnetic properties was confirmed. A localized magnetic moment carried by the Mn ionic cores could not be detected by means of dichroic measurements.

Keywords: Si:Mn, implantation, EXAFS, XMCD, room temperature ferromagnetism

1. Introduction

For decades diluted magnetic semiconductors (DMS) have been extensively investigated in the pursuit of novel ferromagnetic materials, which can be used in spintronic devices. Usually, the Mn-doped III-V and II-VI compounds forming DMS have been in the centre of attention. However, the Si-based DMS have also raised considerable interest, especially after the report that the Mn-implanted Si crystals can be ferromagnetic with a Curie temperature (T_C) higher than 400 K (Bolduc et al., 2005). Main advantage of this material would be the easiness of integrating with the existing technologies and relatively well established procedure to carry out processing at the industrial production. Moreover, the implantation of Mn^+ ions into a silicon matrix would be a good way of exceeding the solubility limit of Mn in Si. On the other hand, the ferromagnetic properties were also reported for silicon samples implanted with non-magnetic ions, e.g. Si or Ar (Dubroca et al., 2006). Therefore, it is important to understand the origin of magnetic properties in this kind of materials. Some authors (Zhou et al., 2007; Yabuuchi et al., 2008) linked the presence of ferromagnetism with the formation of the Mn_4Si_7 nanoinclusions while the others (Misiuk et al., 2006; Osinniy et al., 2008) have not seen this kind of dependence.

A direct way to check whether the magnetism is related to the Mn atom cores is to perform core level X-ray magnetic circular dichroism (XMCD) studies, which allow to detect the local magnetic moments of the specific element what is not possible in the superconducting quantum interference device (SQUID) measurements. Moreover, establishing a correlation between the magnetic properties and the local atomic structure around Mn atoms could also give important indications on the atomic origins of the magnetic properties. In determining the local atomic structure, the X-ray absorption near edge structure (XANES) and extended X-ray absorption fine structure (EXAFS) techniques are extremely useful. Their main advantage is the element selectivity, which allows to extract information on the atomic surrounding of the Mn atoms even at very low concentrations of this element.

2. Experimental

The samples were prepared by Mn^+ implantation into (001) oriented silicon wafers grown by Czochralski (Cz-Si) or by floating zone (Fz-Si) methods. These two silicon single crystals differ in the content of interstitial oxygen atoms. The oxygen concentration was equal to $9x10^{17}$ cm^{-3} for Cz-Si and 1.6 $x10^{17}$ cm^{-3} for Fz-Si. The Cz-Si was doped by B for p-type conductivity and exhibits the resistivity of 12 ohm cm. The Fz-Si was doped by P for n-type conductivity and has high resistivity exceeding 100 ohm cm. The implantation energy of the Mn^+ ions was of 160 keV and a dose of $1x10^{16}$ cm^{-2}. The projected range of the Mn^+ ions was equal to 140 ± 50 nm. The temperature of the Si substrate during implantation was kept at 70°C in the case of Cz-Si:Mn and at 340°C for the Fz-Si:Mn samples. The implanted samples were subsequently annealed at temperatures from 275°C to 1000°C under Ar hydrostatic pressure of either 1 bar or 11 kbar for 1 to 10 hours.

To facilitate this discussion the results for the Cz1-Si samples are also presented. They were prepared in the same manner as the Cz-Si samples. The only difference was that the substrate temperature during the implantation was equal to 340°C, the same as for the Fz-Si case.

The EXAFS measurements at the Mn K-edge were carried out at Hasylab (A1 and E4 stations) using a seven element silicon fluorescence detector. The samples were cooled to liquid nitrogen temperature (LN_2) in order to minimize the thermal part of the disorder. The XMCD spectra at the Mn $L_{3,2}$-edges were measured at MAX-lab (beamline I-1011). The measurements were carried out at room temperature (RT) and also checked at LN_2 temperature under an applied magnetic field of 0.1 T, along the X-ray path. The total electron yield (TEY) detection mode was used. Two angles of X-ray incidence were chosen: grazing (20° to the sample surface) and normal (90° to the surface).

3. Results and discussion

Manganese silicides crystallize in many structures with various Mn to Si ratio, from 3:1 to 1:1.75. In the case of Mn implantation, it is not likely that the formation of inclusions with high Mn content occurs. In order to confirm this assumption, the XANES spectra were analyzed using theoretical calculations. The *ab-initio* calculations were performed using the FEFF 8.4 (Ankudinov et al., 1998). Several phases such as Mn_3Si, Mn_5Si_2 and Mn_5Si_3, as well as the phases with higher Si content were considered. The results of the calculations for two phases: one with a high Mn content - Mn_5Si_2 and one with a low Mn content - $Mn_{15}Si_{26}$ are presented in Fig. 1 as an example. In the Mn_5Si_2 structure, the Mn atoms are located in seven nonequivalent crystallographic positions (Shoemaker and Shoemaker, 1976) while for $Mn_{15}Si_{26}$ the Mn atoms occupy eight such positions (Knott et al., 1967). The FEFF calculations were performed for all the clusters created around each Mn atom in a nonequivalent position and then averaged with the appropriate weight. In Fig. 1 the results of the XANES calculations are compared with an experimental spectrum for one of the samples. The Fz-Si:Mn sample annealed at 800ºC was chosen, however, all the Si:Mn spectra look similar with very broad peaks and lack of sharp features which indicates on the structure with quite high disorder around the absorbing atoms.

As it was expected, the calculated XANES spectrum of the Mn_5Si_2 phase differs significantly from the measured one, while the calculations for the $Mn_{15}Si_{26}$ phase show similarities (Fig. 1). The $Mn_{15}Si_{26}$ phase belongs to the family of the so called higher manganese silicides (HMS), together with the $Mn_{11}Si_{19}$, $Mn_{27}Si_{47}$ and Mn_4Si_7 phases. Their Si/Mn ratio is between 1.70 and 1.75. Their lattice constant *a* is close to 5.5 Å while *c* changes from 17 to 118 Å. A detailed comparison of the lattice parameters can be found in the papers by Zhou et al., 2007 or Migas et al., 2008. Miyazaki et al., 2008 revealed that differences in the HMS composition affect mainly the x and y positions of the Si atoms while it almost does not disturb the Mn sites.

As it was mentioned before, the Mn and Si atoms are located in many nonequivalent crystallographic positions. Twelve such positions were found for Mn in the $Mn_{11}Si_{19}$ phase (Schwomma et al., 1964), eight for Mn in the $Mn_{15}Si_{26}$ phase (Knott et al., 1967; Flieher et

al., 1967), twenty eight for Mn in the $Mn_{27}Si_{47}$ phase (Zwilling and Nowotny, 1972) and five for Mn in the Mn_4Si_7 phase (Gottlieb et al., 2003). EXAFS, similarly like XANES, provides the average information from all of the Mn atoms, therefore, all of them have to be considered in the analysis.

The Artemis and Athena programs (Ravel and Newville, 2005), using the IFEFFIT data analysis package, were applied in the analysis of the EXAFS data. First, the theoretical simulations of the FT spectra for the $Mn_{11}Si_{19}$, $Mn_{15}Si_{26}$, $Mn_{27}Si_{47}$, Mn_4Si_7 phases were performed. Fig. 2 presents simulated spectra which consist of weighted sums of the single scatterings on the Si and Mn atoms located at the distance up to 3 Å around each Mn central atom. In order to show the distribution of the Si and Mn atoms, the scattering paths on all Si near neighbor atoms and next Mn neighbor atoms were summed separately and also included in the Fig. 2. As can be seen, the magnitudes of averaged spheres around Mn atoms look similar. The first peak consists mainly of the Si atoms (8.1 - 8.26 depending on the phase, at average distance ~2.45 Å) while four Mn atoms (~2.97 Å) dominate in the second one. The average atom distribution around the Mn atoms looks very similar for the HMS phases, therefore, it is not possible to distinguish between them by means of EXAFS.

The analysis of the EXAFS spectrum for each investigated Si:Mn sample was carried out in the same way in order to enable the proper comparison between them. We do not observe the influence of multiple atomic excitations on the background, therefore, a linear background was removed from all spectra. During the fitting the simplest model containing one Si path for the first shell and one Mn path for the second one was used. The passive electron reduction factor was fixed to a value equal to 0.75 estimated by the method described in Ravel, 2000 using data of the Cz-Si:Mn sample annealed at 275°C. This factor is strongly correlated with the coordination number (N), therefore, this assumption made possible to find the relative changes in N for the investigated samples in order to monitor the effect of the processing.

Figs. 3 and 4 present the evolution of the magnitude of the Fourier Transformed EXAFS oscillations of the Fz-Si:Mn samples (implanted at 340°C) and Cz-Si:Mn samples (implanted at 70°C) subsequently processed within the range from 275°C to 1000°C (under 1 bar or 11 kbar). One can notice that the local crystallographic environment of the Mn atoms mainly depends on the substrate temperature during the implantation and the annealing temperature, the enhanced pressure seems to be of lesser importance here. However, in some cases the pressure appears to have an impact on the magnetic properties. Nevertheless, the EXAFS spectra did not show any essential differences between the samples produced by annealing under different pressures. For the samples annealed at lower temperatures, up to 450°C for Fz-Si:Mn and up to 340°C for Cz-Si:Mn, only the nearest neighbor shell is clearly detectable. During the annealing at higher temperatures (independently of the applied pressure), the second neighbor shell appears which suggests beginning of the crystallization of the inclusions.

Furthermore, the EXAFS analysis reveals that, for all investigated samples, the first shell consists of silicon atoms and the second shell (in the case it exists) consists mainly of the Mn atoms. The results are presented in the Tables 1 and 2. For all samples the average number of silicon neighbors is between 6 and 8, while the mean distance is around 2.38 Å for

those with the visible second shell and 2.44 Å for those without it. The only exception are the Fz-Si:Mn samples processed at 600°C. In this temperature, the second shell just begins to be formed and it is closer to the first shell than for the other samples.

A similar behavior was observed for the Cz1-Si:Mn samples prepared by implantation at 340°C (Wolska et al. 2007). Some of these spectra are shown in Fig. 5 and the fitting parameters are presented in the Table 3. As can be seen, the second shell starts being formed in effect of processing at 600°C and is clearly visible after processing at 800°C. Therefore, it can be concluded that the differences between the two Si wafers in content of oxygen, in dopants' type (B or P) and in conductivity have no influence on the formation of MnSi inclusions. The inclusions' formation process depends mainly on the temperature of the sample during implantation, not on the type of the substrate.

The X-ray diffraction (XRD) studies of some of the samples (Romanowski et al., 2010) revealed the amorphous phase in the Cz-Si samples implanted at 70°C which partially recovers after processing at 650°C for 10 h but the polycrystalline Si inclusions are still observed. The implantation at 340°C into the Fz-Si substrates resulted in pronounced solid-phase epitaxial re-growth with only few polycrystalline inclusions detectable in the *"as implanted"* sample and after processing the full single crystalline structure is recovered. This fact implies that the existence of structural disorder (e.g. defects at the grain boundaries) in the Cz-Si samples implanted at low temperature makes the diffusion process of the Mn atoms, necessary to form the $MnSi_x$ inclusions, much easier than in the well ordered structure which was formed during the implantation into the warm Fz-Si or Cz1-Si substrates.

In the literature the detected ferromagnetic properties are usually associated with the presence of Mn_4Si_7 inclusions (Zhou et al., 2007; Yabuuchi et al., 2008) and a dependence on the size of the formed inclusions has been observed. The most pronounced magnetic response was observed at liquid helium temperatures and was reported for inclusions with an average size of 11 nm. In the samples with smaller and larger inclusions a very weak magnetic response was found. The size of the inclusions increased with the increase of the annealing temperature. Yabuuchi et al., 2008 reported the existence of at least two kinds of ferromagnetic contributions in the MnSi inclusions and claimed that the magnetic properties cannot be explained by only considering the content of Mn in the inclusions but also the interfaces and other singularities (e.g. band localized at the interface) need to be taken into account.

The SQUID measurements showed that the Fz-Si samples (n-type doping) annealed at temperatures up to 450°C exhibited ferromagnetic properties (Osinniy et al., 2008). For these samples a pronounced solid-phase epitaxial re-growth during implantation was observed (Bak-Misiuk et al., 2009). Therefore, the defects introduced by the presence of separated Mn atoms can be responsible for the ferromagnetic properties. For the Fz-Si sample annealed at 340°C very weak magnetic signal was observed (Romanowski et al., 2010). When the inclusions were formed ferromagnetic properties were not detected.

In the case of Cz-Si samples (p-type doping), such a clear pattern was not found. Some of the samples were antiferromagnetic after annealing at 340°C while others exhibited ferromagnetic properties after annealing at 650°C (Osinniy - private communication). In these samples a high degree of structural disorder is present together with the $MnSi_x$

inclusions up to 650°C, which makes difficult to separate these two factors. Moreover, even after processing at even higher temperature polycrystalline inclusions of Si are still present (Misiuk et al., 2009).

A direct way to check if the Mn ionic cores are responsible for the magnetic properties of the Mn implanted samples is to use XMCD spectroscopy at the Mn L edges. There have been several attempts to measure XMCD in Mn implanted Si but they were unsuccessful. E.g., Orlov et al., 2009 reported on EXAFS and XMCD measurements at the Mn K edge for the sample annealed at 850°C and showed that the Mn_4Si_7 or other similar phases were formed but the dichroic Mn XMCD signal was not observed.

In our case, in agreement with the SQUID results, the samples annealed at low temperatures were taken into consideration. Since the samples exhibited ferromagnetic properties at 300 K, the XMCD measurements at the Mn $L_{3,2}$ edges were conducted at room temperature.

Fig. 6 presents the spectra of the Fz-Si:Mn sample annealed at 275°C under 1 bar, measured for opposite polarities of applied magnetic field. The spectra gathered at the normal and grazing incidence geometries differ in the absorption edge jump but their shape is almost the same (see inset). We do not observe any angular dependence, which indicates that the Mn atoms do not form the ordered layer. There is no intensity difference in the white lines observed after reverting the magnetic field direction, which could be interpreted as a dichroic signal. A dichroic effect did not appear even after cooling the sample to –190^{o}C. The same conclusion can be drawn also in the case of the Cz-Si:Mn sample annealed at 275°C under 1 bar (Fig. 7). This indicates that the Mn atoms are not the source of ferromagnetism in these samples. It is possible that ferromagnetism in the processed Si:Mn samples is mainly related to defects in the Si matrix produced by ion implantation or defects existing at the interfaces between $MnSi_x$ inclusions and the Si matrix. The subsequent thermal processing removes these defects and also, not surprisingly, magnetic properties.

4. Conclusions

Appling the EXAFS technique, the local structure around the Mn atoms was determined in two kinds of Si wafers doped on p and n –type and implanted with Mn at different temperatures and also differently processed. The phases, compositionally related to Mn_4Si_7 were formed around the Mn atoms when the annealing temperature had reached 450°C in the case of Cz-Si:Mn samples implanted at 70°C, whereas a higher temperature was needed for the Fz-Si:Mn samples implanted at 340°C. The applied pressure (1 bar or 11 kbar) did not influence the formation of the inclusions. In case of the Fz-Si wafer, the implantation was conducted into a warm substrate to prevent amorphization and formation of $MnSi_x$ inclusions started at about 600°C. The implantation into Cz-Si wafer was performed at low temperature and lead to amorphization of the substrate as was proved by XRD. In this case the formation of inclusions started already at around 450°C. The existing structural disorder in Cz-Si stimulated the formation of inclusions.

Despite the fact that the structural properties of the vicinity of the Mn atoms clearly depends on the substrate temperature during the implantation and the post implantation

annealing, the magnetic properties do not follow such a clear pattern and do not depend on the kind of doping. Moreover, the XMCD measurements conducted so far did not confirm the presence of a dichroic signal at the Mn ionic cores in spite of clearly observed magnetic response, by means of SQUID magnetometry. This proves the importance of defects in the magnetic properties in Mn implanted Si.

Acknowledgements

The research leading to these results has received funding from the European Community's Seventh Framework Programme (FP7/2007-2013) under grant agreement n°226716. The work at MAX-lab for one of the authors (D. A.) was supported by the Swedish Research Council.

References

Ankudinov, A.L., Ravel, B., Rehr, J.J., Conradson, S.D., 1998. Real-space multiple-scattering calculation and interpretation of x-ray-absorption near-edge structure. Phys. Rev. B 58, 7565-7576.

Bak-Misiuk, J., Misiuk, A., Romanowski, P., Barcz, A., Jakiela, R., Dynowska, E., Domagala, J.Z., Caliebe, W., 2009. Effect of processing on microstructure of Si:Mn. Materials Science and Engineering B 159–160, 99–102.

Bolduc, M., Awo-Affouda, C., Stollenwerk, A., Huang, M.B., Ramos, F. G., Agnello, G., LaBella, V. P., 2005. Above room temperature ferromagnetism in Mn-ion implanted Si. Phys. Rev. B 71, 033302 (4pp).

Dubroca, T., Hack, J., Hummel, R.E., Angerhofer, A., 2006. Quasiferromagnetism in semiconductors. Appl. Phys. Lett. 88, 182504 (3pp).

Flieher, G., Vollenkle, H., Nowotny, H., 1967. Die Kristallstruktur von $Mn_{15}Si_{26}$. Mh. Chem. 98, 2173-2179.

Gottlieb, U., Sulpice, A., Lambert-Andron, B., Laborde, O., 2003. Magnetic properties of single crystalline Mn_4Si_7. Journal of Alloys and Compounds 361, 13–18.

Knott, H.W., Mueller, M.H., Heaton, L., 1967. The Crystal Structure of $Mn_{l5}Si_{26}$. Acta Cryst. 23, 549-555.

Migas, D.B., Shaposhnikov, V.L., Filonov, A.B., Borisenko, V.E., Dorozhkin, N.N., 2008. *Ab initio* study of the band structures of different phases of higher manganese silicides. Phys. Rev. B 77, 075205 (9pp).

Misiuk, A., Bak-Misiuk, J., Surma, B., Osinniy, W., Szot, M., Story, T., Jagielski, J., 2006. Structure and magnetic properties of Si:Mn annealed under enhanced hydrostatic pressure. J. Alloys Comp. 423, 201-204.

Misiuk, A., Barcz, A., Bak-Misiuk, J., Romanowski, P., Chow, L., Choi, E., 2009. Stress-mediated redistribution of Mn in annealed Si:Mn. Materials Science and Engineering B 159–160, 361–364.

Miyazaki, Y., Igarashi, D., Hayashi, K., Kajitani, T., Yubuta, K., 2008. Modulated crystal structure of chimney-ladder higher manganese silicides $MnSi_\gamma$ (γ~1.74). Phys. Rev. B 78, 214104 (8pp).

Orlov, A.F., Granovsky, A.B., Balagurov, L.A., Kulemanov, I.V., Parkhomenko, Yu.N., Perov, N.S., Ganshina, E.A., Bublik, V.T., Shcherbachev, K.D., Kartavykh, A.V., Vdovin, V.I., Sapelkin, A., Saraikin, V.V., Agafonov, Yu.A., Zinenko, V.I., Rogalev, A., Smekhova, A., 2009. Structure, Electrical and Magnetic Properties, and the Origin of the Room Temperature Ferromagnetism in Mn_Implanted Si. Journal of Experimental and Theoretical Physics 109, 602–608.

Osinniy, V., Misiuk, A., Szot, M., Świątek, K., Bąk-Misiuk, J., Barcz, A., Jung, W., Prujszczyk, M., Story, T., 2008. Magnetic properties of silicon crystals implanted with manganese. Materials Science-Poland 26, 751-757.

Ravel, B., 2000. EXAFS Analysis with FEFF and FEFFIT, Part 2, Commentary 37.

Ravel, B., Newville, M., 2005. ATHENA, ARTEMIS, HEPHAESTUS: data analysis for X-ray absorption spectroscopy using IFEFFIT. J. Synchrotron Rad. 12, 537-541.

Romanowski, P., Shalimov, A., Bak-Misiuk, J., Misiuk, A., Caliebe, W., 2010. Structural and magnetic properties of Si single crystals implanted with Mn. submitted to Radiation Physics and Chemistry.

Schwomma, O., Preisinger, A., Nowotny, H., Wittmann, A., 1964. Die Kristallstruktur von $Mn_{11}Si_{19}$ und deren Zusammenhang mit Disilicid-Typen. Mh. Chem. 95, 1527-1537.

Shoemaker, C.B., Shoemaker, D.P., 1976. The Crystal Structure of Mn_5Si_2 and the D Phase (V-Fe-Si). Acta Cryst. B32, 2306-2313.

Wolska, A., Klepka, M.T., Misiuk, A., 2007. Changes in the local structure of the Si:Mn^+ implanted crystals annealed in different temperatures. Hasylab Annual Report 2007, 491-492.

Yabuuchi, S., Ono, Y., Nagase, M., Kageshima, H., Fujiwara, A., Ohta, E., 2008. Ferromagnetism of Manganese–Silicide Nanopariticles in Silicon. Japanese Journal of Applied Physics 47, 4487–4490.

Zhou, S., Potzger, K., Zhang, G., Mücklich, A., Eichhorn, F., Schell, N., Grötzschel, R., Schmidt, B., Skorupa, W., Helm, M., Fassbender, J., Geiger, D., 2007. Structural and magnetic properties of Mn-implanted Si. Phys. Rev. B 75, 085203 (6pp).

Zwilling, G., Nowotny, H., 1972. Zur Struktur der Defekt-Mangansilicide. Mh. Chem. 104, 668-675.

Table 1.
The fitting parameters of the Fz-Si:Mn samples (implanted at 340°C) after different processing and the information on the ferromagnetic properties. N - number of the neighboring atoms, R - distance to the central atom, σ^2 - EXAFS Debye-Waller factor.

Fz-Si:Mn	N	R (Å)	σ^2 (Å^2)	ferromagnetic
275°C, 1 bar	(Si) 6.3±0.5	2.42±0.02	0.009±0.001	yes
275°C, 11 kbar	(Si) 6.7±0.7	2.44±0.03	0.010±0.002	yes
340°C, 1 bar	(Si) 6.7±0.6	2.45±0.03	0.010±0.002	yes
340°C, 11 kbar	(Si) 6.6±0.6	2.44±0.03	0.010±0.002	yes
450°C, 11 kbar	(Si) 7.7±0.5	2.41±0.01	0.011±0.001	yes
600°C, 1 bar	(Si) 6.6±0.5 (Mn) 2.5±0.4	2.37±0.01 2.79±0.01	0.009±0.001 0.013±0.002	no
600°C, 11 kbar	(Si) 6.9±0.8 (Mn) 1.8±1.1	2.39±0.02 2.82±0.03	0.011±0.002 0.010±0.007	no
800°C, 11 kbar	(Si) 7.3±1.0 (Mn) 4.0±1.7	2.37±0.01 2.94±0.01	0.010±0.003 0.007±0.005	no
1000°C, 11 kbar	(Si) 6.3±0.7 (Mn) 3.2±0.8	2.37±0.01 2.92±0.01	0.008±0.002 0.003±0.002	no

Table 2.
The fitting parameters of the Cz-Si:Mn samples (implanted at 70°C) after different processing and the information on the ferromagnetic properties. N - number of the neighboring atoms, R - distance to the central atom, σ^2 - EXAFS Debye-Waller factor.

Cz-Si:Mn	N	R (Å)	σ^2 (Å^2)	ferromagnetic
275°C, 1 bar	(Si) 7.4±0.6	2.43±0.02	0.009±0.001	yes
340°C, 1 bar	(Si) 6.6±1.6	2.45±0.03	0.010±0.004	no
450°C, 1 bar	(Si) 7.3±0.7 (Mn) 3.0±0.9	2.39±0.01 2.94±0.01	0.009±0.001 0.005±0.003	yes
450°C, 11 kbar	(Si) 7.5±0.8 (Mn) 3.0±1.1	2.39±0.01 2.95±0.01	0.010±0.002 0.005±0.003	yes
600°C, 1 bar	(Si) 8.1±1.0 (Mn) 3.0±0.9	2.38±0.01 2.93±0.01	0.012±0.003 0.003±0.002	no
650°C, 11 kbar	(Si) 7.3±0.8 (Mn) 3.6±0.9	2.38±0.01 2.94±0.01	0.009±0.002 0.004±0.002	yes
800°C, 11 kbar	(Si) 7.0±1.3 (Mn) 3.6±1.4	2.36±0.02 2.88±0.02	0.010±0.003 0.003±0.003	no
1000°C, 1 bar	(Si) 6.6±0.8 (Mn) 2.7±0.8	2.37±0.01 2.94±0.01	0.010±0.002 0.002±0.002	no
1000°C, 11 kbar	(Si) 6.3±0.9 (Mn) 4.2±1.3	2.35±0.01 2.94±0.01	0.007±0.002 0.004±0.003	no

Table 3.
The fitting parameters of the Cz1-Si:Mn samples (implanted at 340°C) after different processing. N - number of the neighboring atoms, R - distance to the central atom, σ^2 - EXAFS Debye-Waller factor.

Cz1-Si:Mn	N	R (Å)	σ^2 (Å^2)
340°C, 1 bar	Si 6.5±1.1	2.43±0.02	0.010±0.003
600°C, 1 bar	Si 8.0±1.6 Mn 2.6±0.8	2.41±0.02 2.93±0.03	0.014±0.004 0.008±0.003
800°C, 11 kbar	Si 7.6±1.2 Mn 3.7±1.7	2.37±0.01 2.95±0.02	0.012±0.003 0.007±0.004
1000°C, 11 kbar	Si 7.5±1.3 Mn 3.9±1.8	2.37±0.02 2.94±0.02	0.009±0.003 0.004±0.002

Figure Captions:

Fig. 1.
(Color online) XANES spectra calculated for Mn_5Si_2 and $Mn_{15}Si_{26}$ compared with measured one.

Fig. 2.
(Color online) Theoretical magnitudes of Fourier Transform simulated for $MnSi_x$ phases: a) x=1.72, $Mn_{11}Si_{19}$, b) x=1.73, $Mn_{15}Si_{26}$ c) x=1.74, $Mn_{27}Si_{47}$, d) x=1.75, Mn_4Si_7. Contributions from Si (red dashes) and Mn (blue dots) paths are also shown.

Fig. 3.
Magnitude of the Fourier Transform of the EXAFS spectra and fitting results of the Fz-Si:Mn samples (implanted at 340°C) after different processing. Spectra are shifted vertically for clarity.

Fig. 4.
Magnitude of the Fourier Transform of the EXAFS spectra and fitting results of the Cz-Si:Mn samples (implanted at 70°C) after different processing. Spectra are shifted vertically for clarity.

Fig. 5.
Magnitude of the Fourier Transform of the EXAFS spectra and fitting results of the Cz1-Si:Mn samples (implanted at 340°C) after different processing. Spectra are shifted vertically for clarity.

Fig. 6.
(Color online) XANES spectra of Mn $L_{3,2}$ edges for the Fz-Si:Mn sample annealed at 275°C. Measurements were performed at normal and grazing incidence at RT by inverting the magnetic field direction. In the inset the normalized spectra are shown.

Fig. 7.
(Color online) XANES spectra of Mn $L_{3,2}$ edges for the Cz-Si:Mn sample annealed at 275°C. Measurements were performed at normal and grazing incidence at RT by inverting the magnetic field direction. In the inset the normalized spectra are shown.

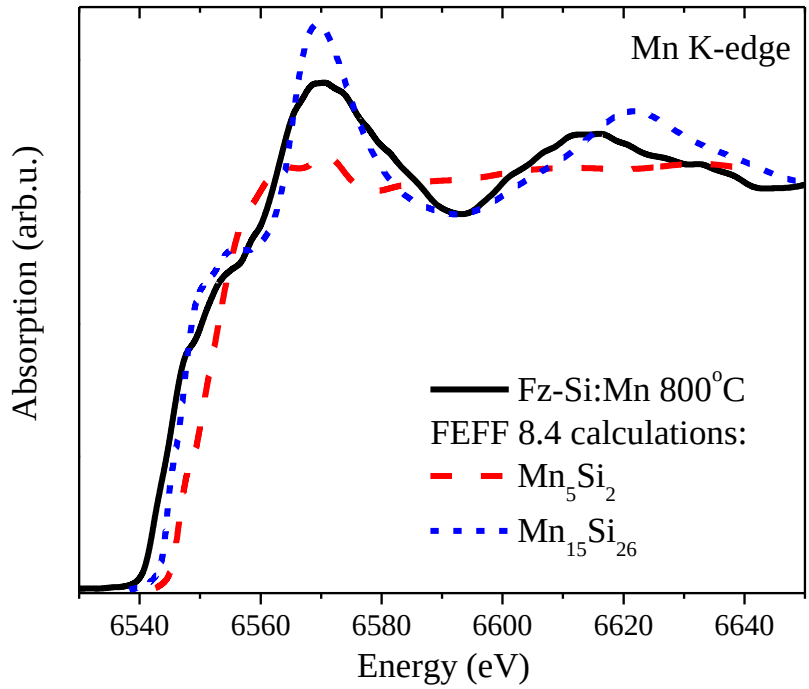
Mn K-edge
Absorption (arb.u.)
Fz-Si:Mn 800°C
FEFF 8.4 calculations:
Mn5Si2
Mn15Si26
6540
6560
6580
6600
6620
6640
Energy (eV)

Fig. 1.

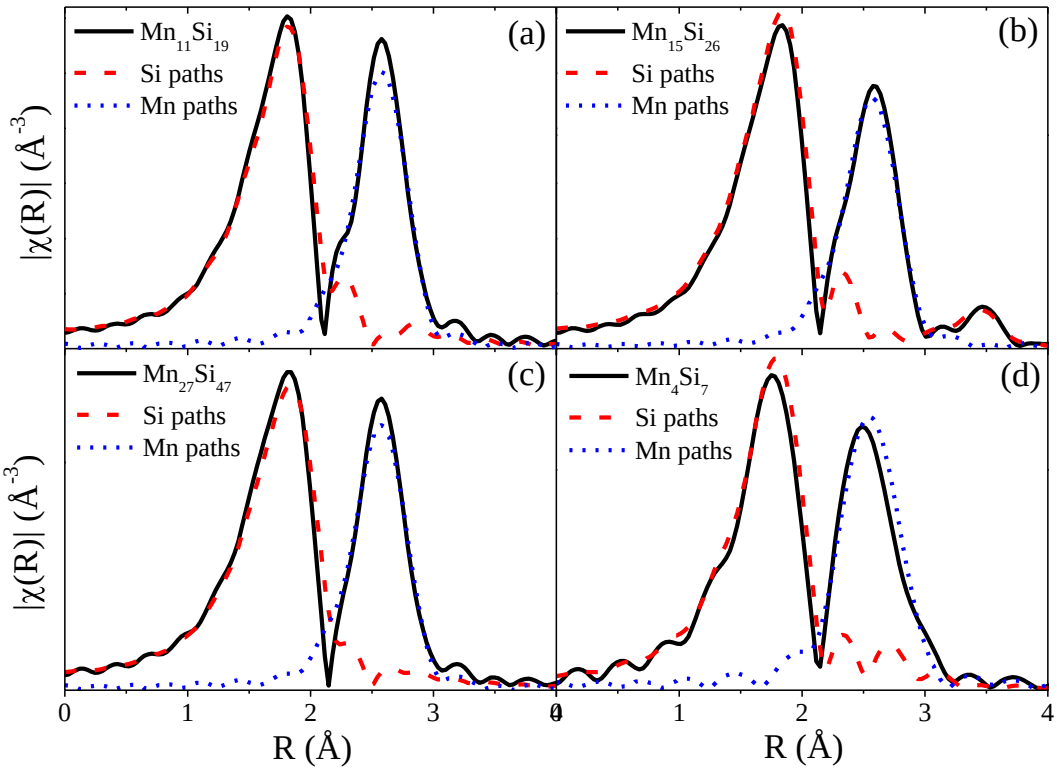
Mn11Si19
Si paths
Mn paths
(a)
Mn15Si26
(b)
Mn27Si47
(c)
Mn4Si7
(d)
|χ(R)| (Å-3)
0
1
2
3
4
R (Å)

Fig. 2.

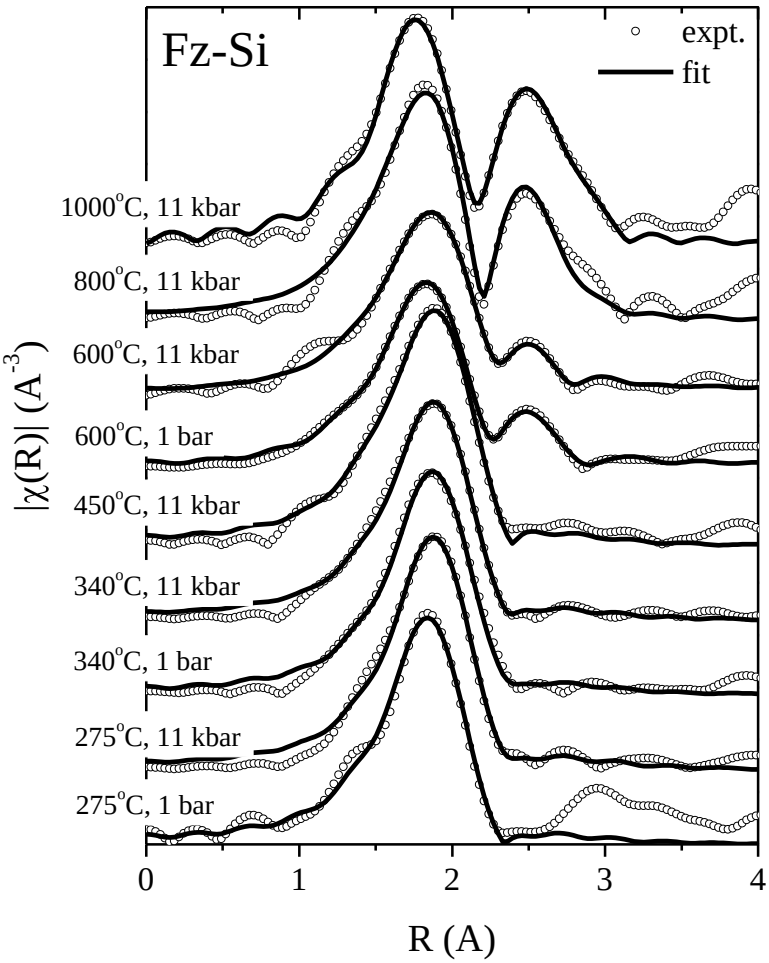
Fz-Si
expt.
fit
1000°C, 11 kbar
800°C, 11 kbar
600°C, 11 kbar
600°C, 1 bar
450°C, 11 kbar
340°C, 11 kbar
340°C, 1 bar
275°C, 11 kbar
275°C, 1 bar
|χ(R)| (A-3)
0
1
2
3
4
R (A)

Fig. 3.

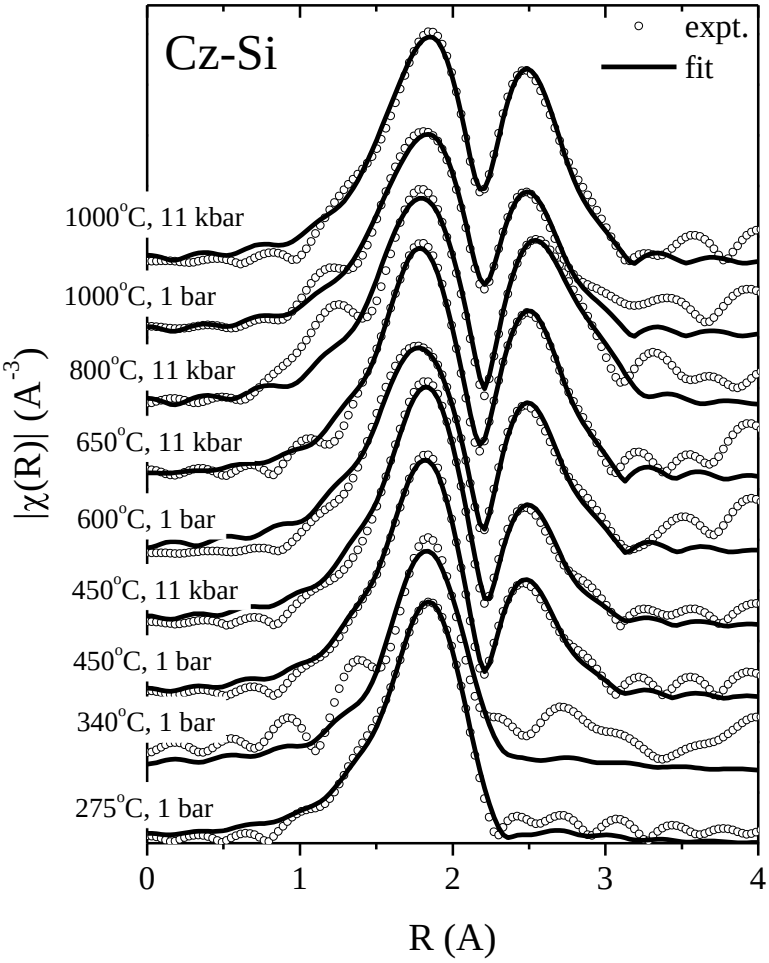
Cz-Si
expt.
fit
1000°C, 11 kbar
1000°C, 1 bar
800°C, 11 kbar
650°C, 11 kbar
600°C, 1 bar
450°C, 11 kbar
450°C, 1 bar
340°C, 1 bar
275°C, 1 bar
|χ(R)| (A-3)
0
1
2
3
4
R (A)

Fig. 4.

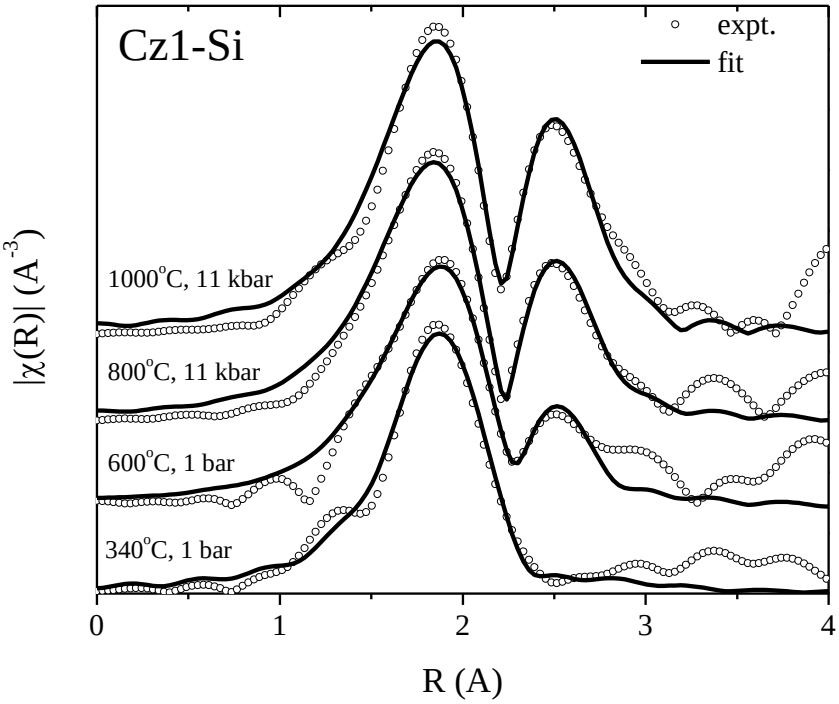
Cz1-Si
expt.
fit
1000°C, 11 kbar
800°C, 11 kbar
600°C, 1 bar
340°C, 1 bar
|χ(R)| (A-3)
0
1
2
3
4
R (A)

Fig. 5.

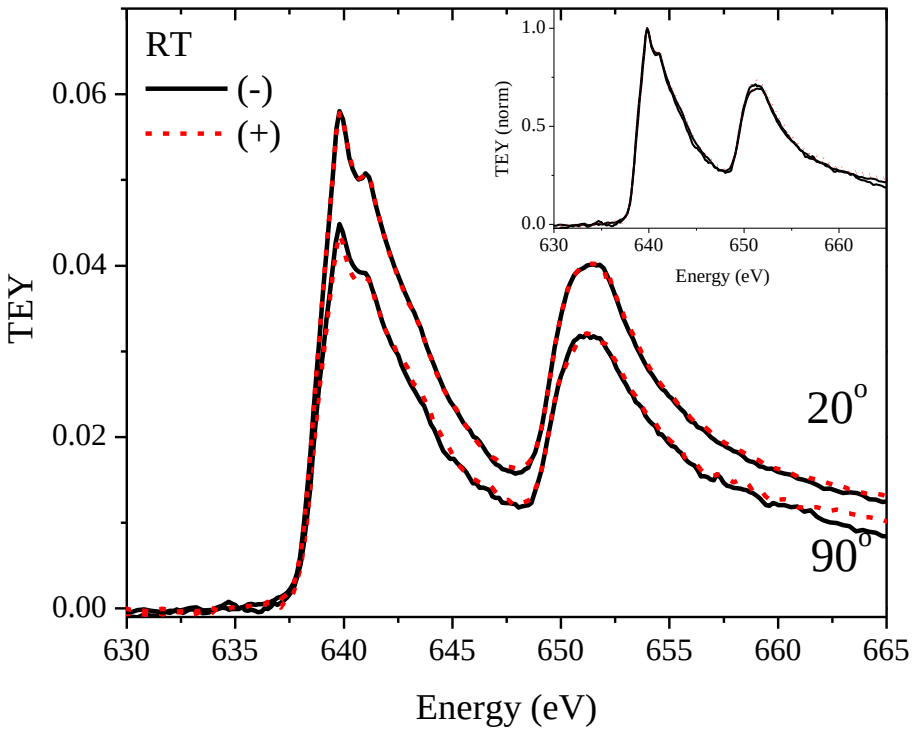
RT
(-)
(+)
TEY
Energy (eV)
20°
90°
TEY (norm)
Energy (eV)

Fig.6.

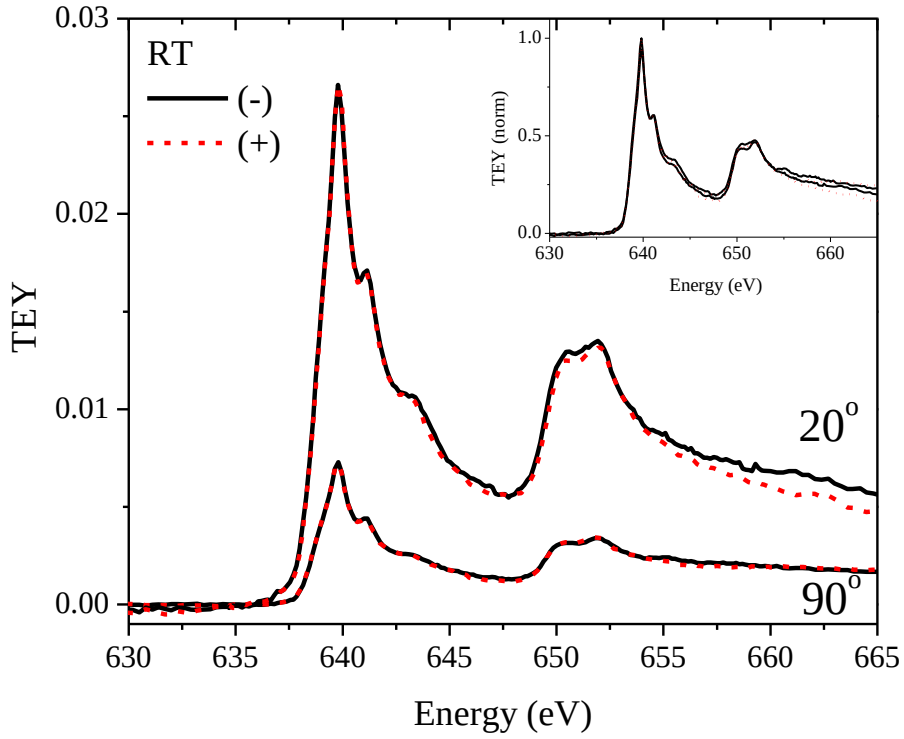
RT
(-)
(+)
TEY
Energy (eV)
20°
90°
TEY (norm)
Energy (eV)

Fig. 2.